Reservoir-Computing for Dispersion Compensation in Digital Filter Multiple Access PON

Yixian Dong, Liang Liu, Yiqian Shi, Xihua Zou, *Senior Member, IEEE*, Wei Pan, and Lianshan Yan

***Abstract*—Chromatic dispersion (CD) is one of the key limitations of increasing the transmission performance for short-reach transmission. The available optical dispersion-compensation techniques are not favored due to their high complexity and other expenses such as power. Reservoir computing is reviewed as a promising technique to provide equalization with memory in an easily trainable fashion, and the properties of the reservoir network are directly linked to system performance. In this article, the digital reservoir computing (RC) based CD-compensation technique is investigated to enhance the transmission performance for digital filter multiple access passive optical network (PON). Numerical results show within 50-km single mode fiber transmission distance for 16 GHz signal bandwidth, the RC-based technique is effective for CD compensation to improve the capacity by 25%.**

***Index Terms*—Reservoir computing, short-reach transmission, multiple access, chromatic dispersion compensation.**

I. Introduction

THE emerging bandwidth-consuming technologies and remarkable applications in current 5G/B5G network are in rapid growth, and these development not only further intensifies the ever-increasing demand for data rates, but also brings a number of other formidable technical challenges including dynamic reconfigurability, flexible and elastic functionality, as well as improved installation/operation cost-effectiveness [1], [2]. To provide a dynamically reconfigurable, flexible, reliable, secure, transparent, smart and high-performance environment to meet these stringent requirements, it is essential to seamlessly converge traditional optical access networks, metropolitan area networks and mobile fronthaul/backhaul networks, which have been separately developed and independently operated over the past a couple of decades. Passive optical networks (PONs) are considered worldwide as one of the most promising candidates for realizing the highly desired network convergence [2].

Digital filter multiple access (DFMA) PONs [3], [4], [5], [6] have recently been proposed for applications in cost-effective software-defined networking (SDN) scenarios, which make use of DSP-based dynamic software reconfigurable digital orthogonal filters to perform channel multiplexing/demultiplexing. The involved digital orthogonal shaping filters (SFs) and matching filters (MFs) are implemented in the digital domain in each individual transceiver in the optical network units (ONUs) and optical line terminal (OLT). Through centralized network resource abstraction and network infrastructure virtualization, the DFMA technique allows multiple independent channels of various signal modulation formats and arbitrary bandwidth granularity to transparently and dynamically share a common fiber transmission medium and other relevant network resources. Both numerical simulations and experimental demonstrations [3], [4], [7] have shown the feasibility of utilizing the technique in cost-sensitive intensity modulation and direct detection (IMDD) DFMA PON application scenarios.

Although DFMA PON provides a promising solution for flexible multiple-user access, its performance is still limited by the chromatic dispersion (CD) along with the loss of phase information in intensity modulation and direct detection (IMDD) [8], [9], in particular for NG-PON2 where the wavelength locates at C-band thus with high dispersion [10]. The available optical CD-compensation techniques are mainly focused on dispersion-compensation fibres (DCFs) [11] or fiber Bragg gratings [12]. Optical domain techniques can fully compensate for the accumulated dispersion, however, due to implementation complexity and high optical power loss, they are not considered for short-reach fibre communications. In contrast to the single carrier modulation such as OOK, PAM, OFDM signal is benefited from its inserted cyclic prefix (CP) in each OFDM symbol, the CP length-endured inter-symbol-interference (ISI) induced by the CD can be effectively compensated [13]. In addition, the OFDM offers an efficient method of dispersion equalization, known as a '1-tap equalizer', which performs a single complex multiplication to real-imaginary pairs to equalize its phase and amplitude [14]. However, the 1-tap equalization and longer CP length cannot solve the problem of RF power fading caused by the CD and direct detection, moreover longer CP come at a cost of data rate within a limited performance. To further satisfy longer transmission with higher bandwidth for future network, massive optical SSB transmission and coherent receiver have been proposed in the literature to eliminate the power fading effect. However, extra optical filter or IQ optical modulator are required, resulting increased cost [15].

For single carrier modulation, such as OOK and PAM-m signal, the digital domain CD-compensation methods including maximum likelihood sequence estimation (MLSE) [16],

Manuscript received 30 August 2023; revised 17 November 2023; accepted 14 December 2023. Date of publication 18 December 2023; date of current version 29 December 2023. This work was supported in part by the China National Key R&D Programmes under Grant 2021YFB2800305, in part by the National Natural Science Foundation of China under Grant 62101465, and in part by the Natural Science Foundation of Sichuan Province under Grant 2022NSFSC0881. *(Corresponding author: Yixian Dong.)*

The authors are with the Center for Information Photonics and Communications, Southwest Jiaotong University, Chengdu 610031, China (e-mail: ydong@swjtu.edu.cn; okarin@my.swjtu.edu.cn; liangmo@my.swjtu.edu.cn; zouxihua@swjtu.edu.cn; wpan@swjtu.edu.cn; lsyan@home.swjtu.edu.cn).

Digital Object Identifier 10.1109/JPHOT.2023.3344115

[17] and Volterra equalization [18], have been demonstrated as promising solutions for CD-compensation. In addition, the machine learning techniques such as artificial neural networks (ANNs) [19], [20] are proposed for CD-compensation. Feed-forward neural networks (FNNs) [21], [22] and recurrent neural networks (RNNs) [23] show promising improvements. FNN system is inherently unable to compensate for CD, as connections between neighboring blocks/neurons are not included. RNNs show property of memory, however, they require back propagating through the full network, thus training parameters are large and the training process is complex. It is therefore desirable to develop schemes where the training phase can be performed with low complexity.

Reservoir computing (RC) offers a novel approach to neuromorphic computing that can considerably reduce the hardware implementation complexity of ANNs, enabling a scalable hardware implementation [24]. RC, also known as Echo State Network (ESN), replaces the hidden layers of NN with a large scale sparsely and randomly connected network (reservoir) [25]. By training partial weights of the network, the training process of the algorithm is greatly simplified, and the shortcomings of the traditional RNN structure are difficult to determine and the training process is too complicated. As a new type of random weight recursive network, it has been proved that RC can reduce the training complexity of NN and improve the performance of optical communication system. In [24], [26], [27], RC has been studied in single carrier modulation such as OOK and PAM-m in short reach optical transmission. In this work, RC is utilized for the first time in the uplink of DFMA PON with multicarrier modulation in multiple user access application scenarios. To obtain the phase variation-induced amplitude changing information, RC is applied before L-downsampling in the receiver of DFMA PON link. Numerical simulation results manifest that digital RC is feasibility for the uplink of DFMA PON. Comparing to the CD-compensation free system, the CD-destroyed channels can reach HD-FEC limit of BER at 3.8×10^{-3}.

The main contributions of this article can be summarized as follows:

- To explore the effectiveness of digital RC method for CD-compensation, different RC parameters are explored, including reservoir size, spectral radius, leaking rate, and sparsity.
- The key digital filter parameters including roll-off factor and filter length in DFMA PON are investigated for both RC-compensated and no-compensation channels.
- For fixed digital filter parameter and RC parameter, uplink transmission performance is compared between RC-compensation and non-compensation channels. Moreover, the total capacity, transmission length, the receiver sensitivity and the differential optical launch power are also calculated.

The remainder of this article is organized as follows. In Section II, we describe the model of a general DFMA PON with digital RC implemented in the receiver DSP. Meanwhile, the details of RC implementation is introduced. In Section III, simulation results are presented and discussed in aspects of RC parameters, digital parameters and transmission performance. Section IV concludes this work.

II. System Model

A. Upstream of DFMA PON

The schematic diagram of the IMDD DFMA PON is depicted in Fig. 1. The digital orthogonal filtering for multiplexing/demultiplexing downstream/upstream signals are employed in the digital domain. For the downstream, the signal can be multiplexed in the digital domain, the same as in the point-to-point transmission system [28], and digital RC can be easily adopted in the RX DSP, as shown in Fig. 1. In this article, special attention is given to the multipoint-to-point upstream operation only.

For the upstream operation, the ith ONU data digitally encoded by an arbitrary signal modulation format is upsampled ($L\uparrow$) by a factor of L via inserting L-1 zeroes between two consecutive original data samples. The upsampled data sequence is subsequently passed through a digital shaping filter (SF). Having been digitally filtered, the resulting data sequence is passed through a digital-to-analog converter (DAC) and an optical intensity modulator (IM) to generate the optical signal. Different optical signals from various ONUs attached to the DFMA PON are finally passively combined by a coupler in the remote node and propagated through the fiber transmission link to the OLT. An example of how different orthogonal filters are assigned to individual ONUs is illustrated in the inserted figure of Fig. 1, where the gapless frequency responses of both I and Q components of these Hilbert-pairs at different central frequencies are plotted. Here, the signal from ONU1 and ONU2 share the same central frequency. In the OLT, after a photodetector (PD) and an analog-to-digital converter (ADC), the data stream corresponding to the ith ONU can be demultiplexed by the corresponding matching filter (MF), whose coefficients are computed by the OLT-embedded DSP controller following a procedure similar to its ONU counterpart. For the CD-compensation transmission scheme, the digital RC is applied before the downsampling ($L\downarrow$), which selects every Lth sample. Finally the ith ONU data is recovered after decoding.

The construction of various digital orthogonal SF and MF filters employed in the ONUs and OLT is undertaken using the Hilbert-pair approach, and the impulse responses of the ith in-phase and quadrature-phase filter components, represented by "I" and "Q", respectively, $g_i^w(t)$, (w= I and Q), can be written as:

$$g_i^w(t) = \begin{cases} p(t)\cos\left(2\pi f_{ci} t\right) w = I \\ p(t)\sin\left(2\pi f_{ci} t\right) w = Q \end{cases} \tag{1}$$

where f_{ci} corresponds to the central RF frequency of the ith Hilbert-pair and $p(t)$ is the baseband pulse having a square-root raised-cosine form given by

$$p(t) = \frac{\sin\left[\pi\left(1-\alpha\right)t'\right] + 4\alpha t' \cos\left[\pi\left(1+\alpha\right)t'\right]}{\pi t'\left[1-\left(4\alpha t'\right)^2\right]}, t' = \frac{t}{T} \tag{2}$$

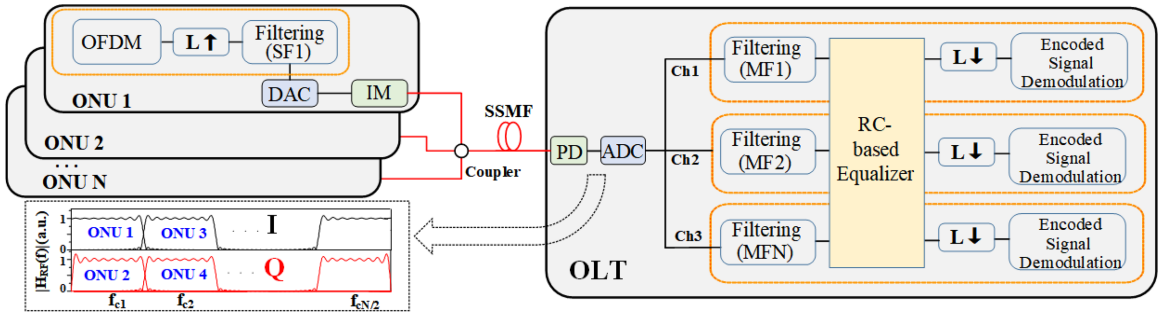

Fig. 1. Schematic of the IMDD based upstream DFMA PON transmission system. Inserted figure: An example of different orthogonal filters assigning to individual ONUs, where the gapless frequency responses of both I and Q components of these Hilbert-pairs at different central frequencies.

where T is the symbol period prior to up-sampling and the α parameter controls the excess of bandwidth of the square-root raised-cosine function. Each of these filter components can be independently utilized to convey an individual signal, thus represents an independent channel. The impulse response of the ith SF ($s_i(t)$) in the ith ONU, and the jth MF($m_j(t)$) in the OLT satisfies the following relationship

$$\begin{cases} s_i(t) = g_i^w(t) \\ m_j(t) = g_j^w(-t) \end{cases} \quad w = I \text{ or } Q \tag{3}$$

with

$$s_i(t) \otimes m_j(t) = \begin{cases} \delta(t - t_0) & i = j \\ 0 & i \neq j \end{cases} \tag{4}$$

where t_0 corresponds to the total time delay induced by the digital filtering process. For an optical signal of a specific wavelength transmitting N independent channels, the central RF frequency of the ith Hilbert-pair, f_{ci}, is governed by

$$f_{ci} = (2i - 1)\frac{f_{DAC/ADC}}{2N} i = 1, 2, 3, \cdots, \frac{N}{2} \tag{5}$$

where $f_{DAC/ADC}$ is the sampling rate of the DAC/ADC.

Thus, a DSP-enabled dedicated physical connection between the ith ONU and the OLT is established, which fully supporting the SDN solution, and greatly easing transparent abstraction and virtualization processes because of inherent rich DSP-enabled network intelligence.

B. Digital Reservoir Computing

The digital RC adopted in this article is illustrated in Fig. 2, which mainly includes the input layer, reservoir, and output layer. The input signal vector $\mathbf{u}[n] = [u_1[n], \ldots, u_N[n]]^T$ consists of a real N-dimensional vector at the discrete-time instant n, where N represents the number of inputs. The output layer uses a linear activation function to linearly combine the neurons in the reservoir to output the recovered signal, $\mathbf{y}[n] = [y_1[n], \ldots, y_K[n]]^T$ is expressed as :

$$\mathbf{y}[n] = \mathbf{W}_{res}^{out} \cdot \mathbf{x}[n] + \mathbf{W}_{in}^{out} \cdot \mathbf{u}[n] \tag{6}$$

where $\mathbf{x}[n]$ is the states of reservoir ($\mathbf{x}[n] = [x_1[n], \ldots, x_M[n]]^T$), including M of reservoir nodes. $\mathbf{W}_{res}^{out}$ defines the weights and interconnection between the M reservoir states and the K network outputs, while $\mathbf{W}_{in}^{out}$ describes a direct

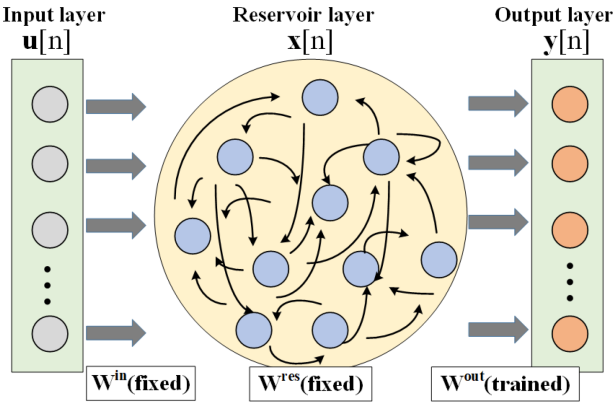

Fig. 2. Reservoir computing schematic for CD compensation.

connection between input and output layers. The evolution of the reservoir $\mathbf{x}[n]$ at the time instant n is a function of input and the previous time:

$$\mathbf{x}[n] = \beta \cdot f_{act}(\mathbf{W}^{in} \cdot \mathbf{u}[n] + \mathbf{W}^{res} \cdot \mathbf{x}[n-1]) + (1 - \beta) \cdot \mathbf{x}[n-1] \tag{7}$$

where β is the leakage rate to emulate an exponential decay within the reservoir, to satisfy the echo state property and mimic realistic physical implementations. $\mathbf{u}[n]$ is injected into the reservoir through a linear transformation given by the $M \times (N + 1)$-dimensional $\mathbf{W}^{in}$, where $N + 1$ takes into account a bias component.

The key advantage of the RC approach relies on the fact that, once a suitable $M \times M$-dimensional $\mathbf{W}^{res}$ is constructed, the evolution of the reservoir states depends only on the inputs, and training is only applied to optimize the output weights ($\mathbf{W}_{res}^{out}, \mathbf{W}_{in}^{out}$). Such an optimization does not require the complex and computationally expensive back-propagation through the whole network, as is the case for RNNs (back-propagation-through-time algorithm) or even simpler FNNs (back-propagation algorithm). The training can be performed with a single linear regression operation, possibly with ridge regularization included, aiming at minimizing the squared error of the loss function.

Generally, the training process of RC includes two stages: states selection and weights calculation. In the state selection

stage, the initial state of the reservoir needs to be determined first, and the initial state is usually assumed to be 0. The update process of the state is shown in (7). $\mathbf{W}^{in}$ and $\mathbf{W}^{res}$ are randomly generated (satisfying uniform or normal distribution) and kept constant throughout the training phase. In the weights calculation stage, the matrix $(\mathbf{W}_{res}^{out}, \mathbf{W}_{in}^{out})$ needs to be calculated according to the collected system state matrix A and training data, so that the actual output of the network is close to the expected output result. As shown in

$$\mathbf{Y}_{\text{target}} = (\mathbf{W}_{res}^{out}, \mathbf{W}_{in}^{out})^{\mathrm{T}} \cdot \mathrm{A} \tag{8}$$

To make the error between $\mathbf{Y}_{\text{target}}$ and $\mathbf{Y}$ as small as possible, we define the mean squared error (MSE) as the target loss function in the training phase and solve this linear regression problem using the least squares method. Computationally, this problem can be further processed as a pseudo-inverse problem of A.

$$(\mathbf{W}_{res}^{out}, \mathbf{W}_{in}^{out}) = (\mathrm{A}^T \cdot \mathrm{A} + \lambda \mathbf{I})^{-1} \cdot \mathrm{A}^T \cdot \mathbf{Y}_{\text{target}} \tag{9}$$

In (9), we use ridge regression to process A. The stability and reliability of traditional least square is improved by adding a regularization term (λ). The completion of $\mathbf{W}^{out}$ calculation represents the end of RC training process.

C. Reservoir Computing-Based Equalization

For the upstream DFMA PON, the signal sampled by the ADC in the OLT is originally effected by the CD effect, and the signal after L-downsampling is obtained by selecting every L-th sample, which may lose temporal information interference. While RC-based compensation is highly dependent on the temporal information processing with memory, thus the signal after matching filter but before L-downsampling is utilized for RC-based equalization. The training sequence in the transmitted signal is utilized for RC-based training process, and it will go through the whole channel effect, including filtering effect and CD. To keep consistent with the received training signal, the target signal from the transmitter also go through shaping and matching filter process. Thus, the training signal is a matrix $\in \mathrm{R}^{N \times \mathrm{J}}$, the row N represents the ONU or channel number, J is the training length of each channel. For the states selection, all the input and reservoir weights are drawn for a uniform distribution $\mathcal{U}$(-1,1). Concerning f_{act}, $\tanh(\cdot)$ is considered in this work. The reservoir interconnections are with the probability of no interconnection $p(w_{ij}^{res} = 0)$ corresponding to the desired degree of sparsity or connectivity of the reservoir matrix. In addition, the spectral radius ρ defined as the maximum eigenvalue of $\mathbf{W}^{res}$ is a key hyper-parameter, affecting the RC stability. To explore the expected behavior of the reservoir, the spectral radius, leakage rate, sparsity and reservoir size are studied in the next section.

III. System Performance

In this section, we evaluate and compare the performance of upstream DFMA PON transmission with and without RC-based CD compensation. To emphasize the CD compensation effect, fibre nonlinearity is neglected for the low optical launch power

TABLE I
Power Allocation Strategy

Parameter	Value	Parameter	Value
DAC/ADC Sampling Rate	32 GS/s	Upsampling factor L	4
IFFT size of OFDM signal	32	Cyclic prefix of OFDM signal	0.25
Clipping ratio	14 dB	ENOB (effective NO. of bits)	8 bit
Optical launch power	1 mW	CW operation frequency	193.1 THz
Fiber dispersion	16.4×10^{-6} s/m^2	Fiber dispersion slope	0.08×10^{3} s/m^3
The quantum efficiency	0.8	Fiber length	20 km
Reservoir size	400	Spectral Radius of RC	0.9
Leakage rate of RC	0.99	Sparsity of RC	0.25
Regularization of RC	1×10^{-8}	Training/ Transmitted symbol	2458/819

in PON application scenario. The chromatic dispersion are considered with group velocity dispersion (GVD) parameter and second-order GVD parameter [13], and the dispersion parameters are listed in Table I. Both signal generation, detection and fibre dispersion effect are simulated using MATLAB software. To simulate the OFDM signal generation and detection, the approach reported in [6] is adapted. Throughout the article, each ONU is assigned with a whole real-valued OFDM channel, with each channel consisting of fifteen, 16-QAM modulated, data-bearing subcarriers (IFFT size is 32) if without any special note. In each ONU, an ideal optical intensity modulator is utilized, which produces an optical field signal expressed as:

$$E_o(t) = \sqrt{1 + m \cdot y'(t)} \tag{10}$$

where m is the modulation index, $y'(t)$ is the electrical driving signal.

Apart from simplicity, the utilization of the ideal optical intensity modulator can also completely eliminate the optical beat interference (OBI) effect. For simplicity but not losing generality, four ONUs are considered in the adopted multipoint-to-point upstream PONs. The construction of the digital filters in the ONUs is undertaken using the Hilbert-pair approach [6], in which the baseband pulse has a square-root raised-cosine form and the central frequency f_k corresponds to the RF central frequency of the Hilbert-pair. Each Hilbert-pair includes both in-phase and quadrature-phase filter components to support two spectrally-overlapped orthogonal channels. In this article, upsampling factor L is taken to be 4, and the two central frequency are $f_1 = f_s/8$, $f_2 = 3\ f_s/8$, f_s is the DAC/ADC sampling speed.

After direct detection, the detected electrical signal $I(t)$ is

$$I(t) = |E_o \otimes h(t)|^2 = [E_o \otimes h(t)] \cdot [E_o \otimes h(t)]^* \quad (11)$$

where $h(t)$ is the channel response. When only dispersion is considered, the channel transfer function in frequency domain is

$$H(f) = e^{j\Phi_D}, \Phi_D = 2\pi^2 \beta_2 L f^2 \quad (12)$$

where Φ_D is the chromatic dispersion-induced phase shift, f indicates the signal frequency offset with respect to the optical carrier, and β_2 is the group velocity dispersion. For a simply clarification in this part, only GVD parameter is considered in the fiber dispersion of (12).

Expanding the detected signal $I(t)$ in Taylor series, The optical signal can be approximated by

$$E_o(t) = \sqrt{1 + m \cdot y^{'}(t)} = \sqrt{1+X}$$
$$= 1 + \frac{1}{2}X - \frac{1}{8}X^2 + \cdots, X = m \cdot y^{'}(t) \quad (13)$$

Considering the channel response, the square-law detected signal can be expanded as

$$I(t) = 1 + X \otimes \frac{h(t) + h^*(t)}{2} - X^2 \otimes \frac{h(t) + h^*(t)}{8} + \cdots \quad (14)$$

The second term of (14) is the desired signal with IMDD system channel response. Combining (12) and (14), the IMDD system transfer function in frequency domain is

$$H^{'}(f) = \frac{H(f) + H^*(f)}{2} = \cos(2\pi^2 \beta_2 L f^2) \quad (15)$$

Therefore, the optical dispersion effect is not linearly mapped into electrical domain, and such damage cannot be equalized by the '1-tap equalizer'. Fig. 3(a) shows each ONU location in the spectral, and ONU3 and ONU4 are overlapped in the higher RF frequency range. It can be seen that the power fading is shown around the frequency range [13 GHz,15 GHz], and the corresponding subcarriers (index 7 to index 11) are badly destroyed, thus these subcarriers are dropped in the following discussion. While after RC-based CD compensation, the RF fading effect is significantly mitigated and the spectral is more flat than that without RC compensation, as shown in Fig. 3(b).

A. The Optimum RC Hyper Parameter

All the key simulation parameters are listed in Table I, and the OFDM signal of each ONU is sampled at 32 GS/s and transmitting 20 km of fibre with dispersion effect. The received optical power is set to be -2 dBm to guarantee the transmission system having a reasonable SNR. Due to the accumulated dispersion, ONU3 and ONU4 located at higher frequency range is badly destroyed in the IMDD system. To overcome the dispersion effect, the digital RC-based equalization is implemented in the receiver, and its key hyper-parameters are listed in Table I. The reservoir size or the RC nodes is selected to be 400. Since the larger the RC nodes, the more complex the RC-induced implementation complexity. Moreover, the system performance depend on the reservoir size is explored in Fig. 4(a). For the most

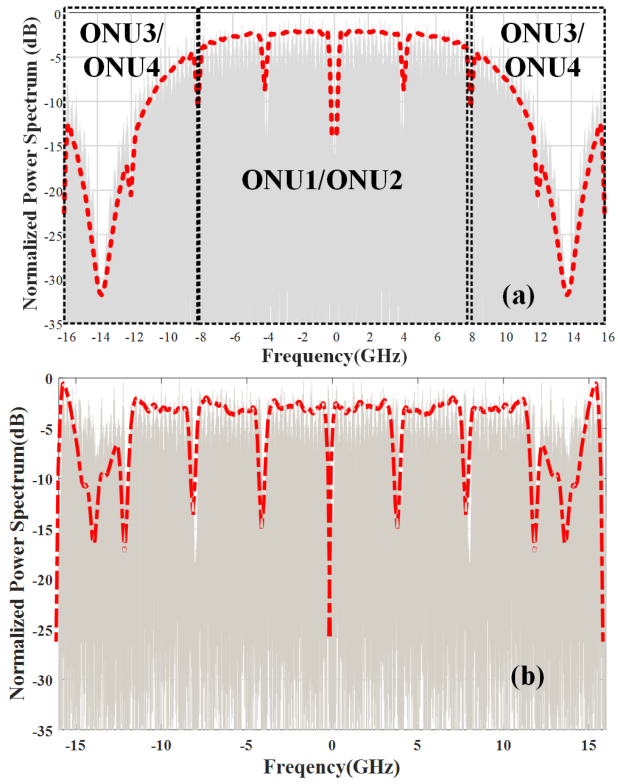

Fig. 3. Normalized power spectrum of the received signal after PD (a) before RC compensation. (b) After RC compensation.

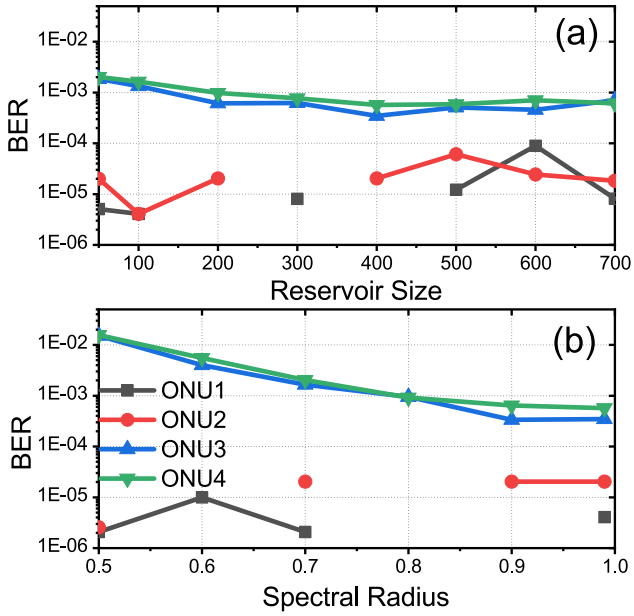

Fig. 4. (a) BER vs reservoir size. (b) BER vs reservoir radius.

CD-effected channels ONU3 and ONU4, their performance is improved by increasing the reservoir size, and reach the lowest BER after the size of 400. When the size is larger than 400, the performance tends to be stale. Meanwhile, the performance of ONU1 and ONU2 located at the lower frequency range is less effected by the dispersion, and the reservoir size have little

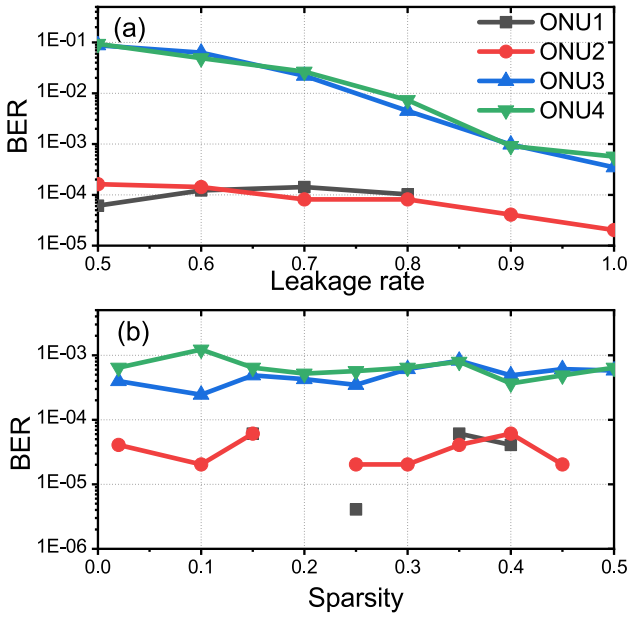

Fig. 5. (a) BER vs reservoir leakage rate. (b) BER vs reservoir sparsity.

impact on their performance. Since limited signal samples are utilized, the BER variation below 1×10^{-4} is resulted from the statistical error.

In addition to the reservoir size, the spectral radius is defined as the absolute value of the largest eigenvalue of the connection weight matrix $\mathbf{W}^{res}$, which is a key parameter to ensure the stability of the algorithm. When spectral radius is less than 1, the network has the property of echo. In Fig. 4(b), the performance of ONU3 and ONU4 improves with increasing the spectral radius. This is because the increased spectral radius leading to larger reservoir memory, and the reservoir increases its ability to invert the memory effect in the transmission channel.

In (7), the leakage rate β is utilized to mimic realistic physical implementation, and its impact on the performance of RC is also explored. As shown in Fig. 5(a), by increasing the leakage rate, the performance of the algorithm is significantly improved. In the range of 0.9 to 1, the performance tends to be stable. When the leakage rate is 1, the leaky integral neurons degenerate into ordinary neurons. Theoretically, leaky integral neurons can improve the performance of the reservoir. Without loss of generality, the values of spectral radius and leakage rate are 0.9 and 0.99, respectively.

Moreover, the sparsity represents the proportion of non-zero elements to the total elements in the neuron connection matrix of the reservoir. Generally, the smaller the sparsity is, the simpler the internal structure of the reservoir is. A brief analysis of the impact of such hyper-parameter has shown a minimal impact on system performance [24], this is also confirmed in Fig. 5(b). From the range 0.02 to 0.5, the sparsity has little effect in the performance of the digital-RC based equalization. Here, sparsity of 0.25 is chosen for the following study. Thus, we have identified all parameters that affect the computational performance of the reservoir, and applied to the following study.

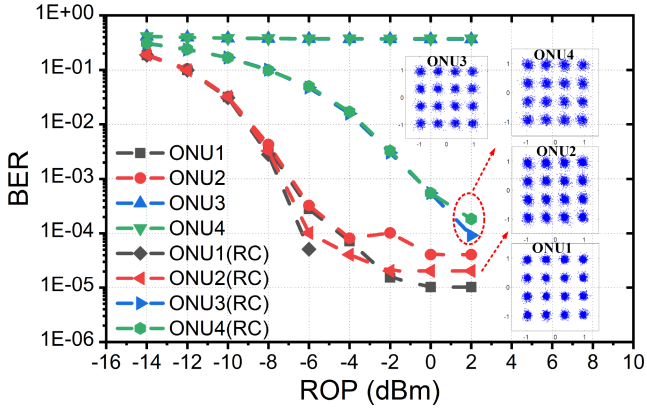

Fig. 6. BER vs received optical power (dBm).

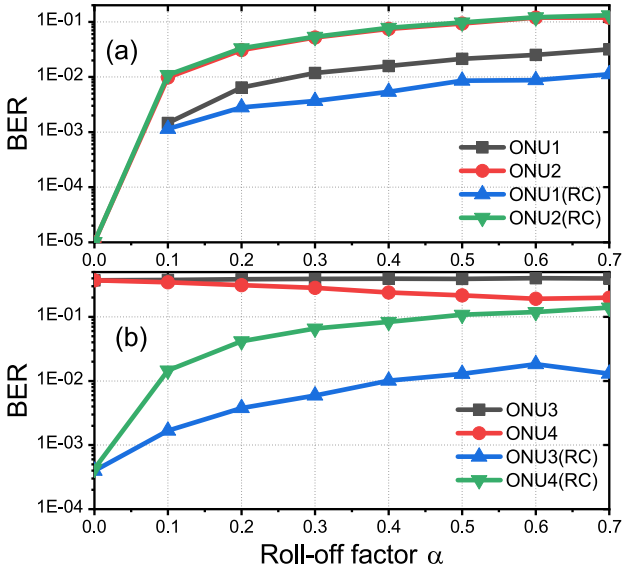

Fig. 7. BER vs shaping/matching filter roll-off factor α.

B. RC-Improved Performance Dependence on Filtering Effect

Applying with the identified optimum parameters in the previous section, the BER versus received optical power (ROP) of the upstream transmission of DFMA PON is illustrated in Fig. 6. It is clear that without any dispersion compensation, the corresponding ONU3 and ONU4 fail to work. After applying with the RC-based compensation, both the two channels reach to HD-FEC limit of BER at 3.8×10^{-3} when the received optical power is larger than -3 dBm. At the ROP of 2 dBm, each ONU's corresponding constellations after RC are shown in Fig. 6, it is clear that the quadrature channels (ONU2/ONU4) are still effected by the filtering effect [28].

Thus, Fig. 7 presents the four ONU performance versus ROP for different levels of adjacent channel interference (ACI). Here the different ACI levels are introduced by varying the filter's alpha parameter [29], which controls the excess of bandwidth with respect to the minimum bandwidth determined by the symbol period. Generally speaking, for a given filter tap count, a larger alpha value produces lower in-band frequency response

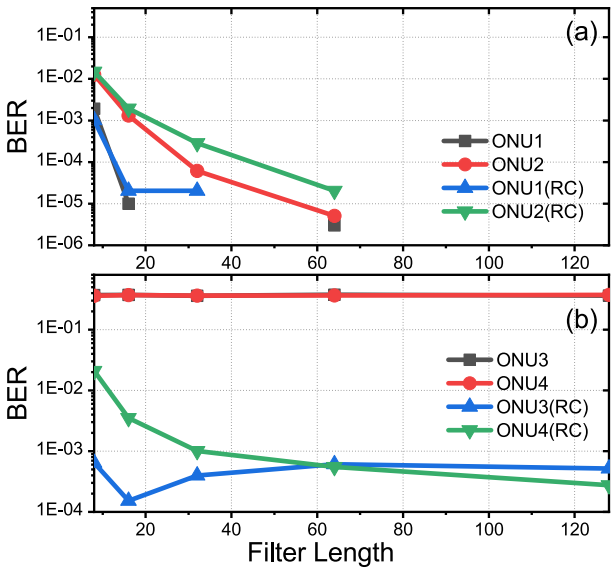

Fig. 8. BER vs shaping/matching filter length.

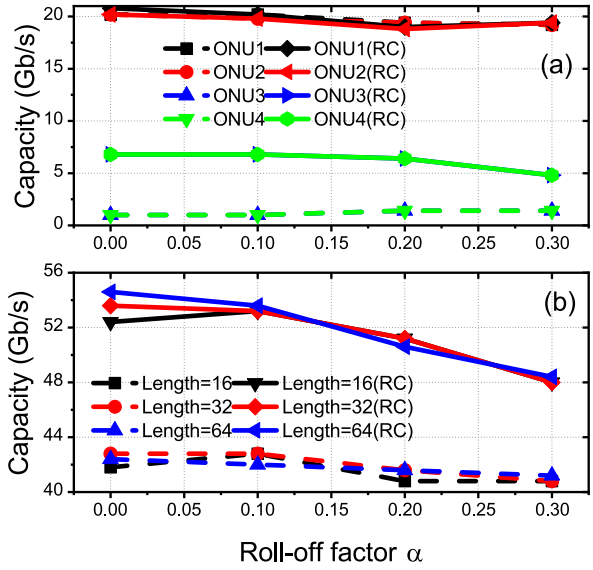

Fig. 9. (a) Each ONU capacity vs filter roll-off factor with/without RC at length of 64. (b) Aggregated capacity of all four ONUs vs filter roll-off factor at different filter length.

ripples, but gives rise to larger filter response side lobes, thus leading to greater ACI. Varying the roll-off factor α from 0 to 0.7 while fixing the filter length at 32, the transmission performance of BER is compared in Fig. 7. For the dispersion effected channels ONU3 and ONU4, RC-based compensation greatly reduced the BER. In addition, the quadrature channel ONU4 shows less improvement than that of ONU3, this is due to the quadrature channel ONU4 enduring more oscillating structure than in-phase channel of ONU3. This is also confirmed in ONU1 and ONU2, where the RC-based technique cannot compensate the oscillating-induced signal damage.

In addition, fixing the roll-off factor at 0.001, varying the filter length from 8 to 128, Fig. 8 shows that the RC-assisted transmission performance of ONU3/ONU4 is improved and reach stable at the filter length of 32. The performance degradation at length smaller than 32 is because that more error of the received data leads to the invalid of RC training. The results above indicate that the filtering-induced signal distortion cannot be equalized by RC.

C. RC-Improved Performance on DFMA PON

To explore the RC-enhanced transmission capacity, each ONU and the aggregated transmission capacity of the DFMA PON are shown in Fig. 9. The aggregated signal transmission capacity for a fixed DAC/ADC sampling speed is achieved by the adaptive bit loading applied to each subcarrier, and the capacity of each ONU/channel is calculated by (16)

$$R_b = \frac{f_s \sum_{k=1}^{N_s} n_{kb}}{(\text{FFT\_size})(1+C_p)L} \tag{16}$$

where n_{kb} is the number of binary information bits conveyed by the k-th subcarrier within one OFDM symbol period, C_p is the overhead parameter associated with the cyclic prefix.

Applying with the RC parameter from previous section, from Fig. 9(a), it is clear that the capacity of ONU3/ONU4 is enhanced from 1 Gb/s to 6.8 Gb/s after 20-km fibre transmission when α is in the range of [0, 0.2]. For ONU1 and ONU2, their capacity is kept stable with and without RC-based CD-compensation. In Fig. 9(b), the aggregated capacity with four ONUs is presented with variations of digital filter roll-off factor and filter length at 16, 32 and 64. For $\alpha = 0$, more than 25% aggregated capacity is booted for different filter length. As the ACI increased, the capacity enhancement slower down. Moreover, the filter length-induced capacity improvement is small compared to RC-induced capacity improvement, thus the curves with different filter length are almost overlapped.

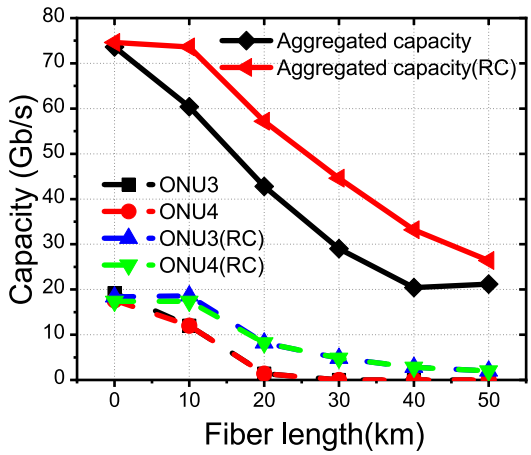

Fig. 10. Capacity vs transmission fiber length.

Additionally, the aggregated capacity along with the fibre length is presented in Fig. 10. It can be seen that the without any CD-compensation, the maximum reach of ONU3/ONU4 is 30 km at such high DAC/ADC sampling speed of 32GS/s, and RC-based compensation technique can boost reach to more than 50 km, even though the capacity improvement is decreased with

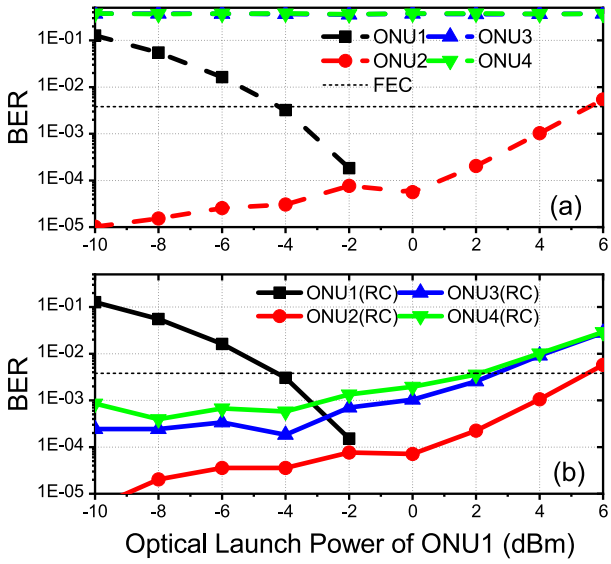

Fig. 11. BER performance vs ONU1 optical launch power.

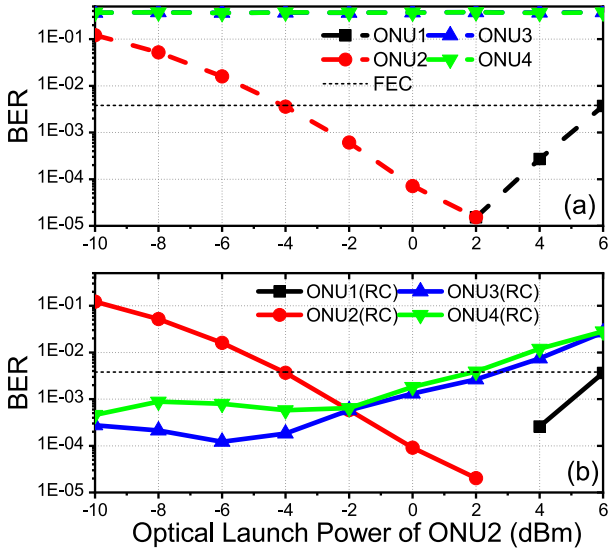

Fig. 12. BER performance vs ONU2 optical launch power.

accumulated dispersion. For the aggregated capacity containing all four channels, the average capacity increment is 13 Gb/s from 10 km to 40 km of fibre length. When increasing fiber length to more than 50 km, the limited CD-compensation of digital RC shows little transmission improvement brought to the DFMA PON.

D. Differential Optical Launch Power Range

The RC-assisted DFMA-PON performance robustness to differential ONU launch power is examined in Figs. 11 and 12, where the BER performance of a power-varying ONU is plotted as a function of its optical launch power, whilst the other fixed-power ONU's launch power is kept constant at 0 dBm. For simplicity but without losing generality, here four ONUs are considered and the ROP in the OLT is fixed at −2 dBm. The digital filters have 32 taps, and the alpha parameters are set at 0. All other parameters are identical to those listed in Table I.

As expected, an increase in optical launch power from one ONU improves its own BER performance, but simultaneously degrades the BER performance of the other ONU, as shown in Figs. 11 and 12. This mainly results from the opposite changes in effective optical signal to noise ratio (OSNR) experienced by these ONUs. In this context, the differential ONU launch power dynamic range is defined, for a fixed ROP in the OLT, as the maximum allowable variation range of optical launch power from a specific ONU, over which the total BERs of all individual ONU signals simultaneously transmitted over the PON are still less than the adopted FEC limit.

At an ROP of −2 dBm, ONU3 and ONU4 are failed to work with increasing launch power of ONU1 or ONU2 in Figs. 11(a) and 12(a), while the differential launch power dynamic range of the RC-assisted DFMA PON can be extended to 6 dB in Figs. 11(b) and 12(b). Such a huge improvement mainly results from the ONU3 and ONU4 performance improvement helped by digital RC-based equalization. The enhanced differential ONU dynamic range also brings improved PON performance robustness. Meanwhile the differential launch power dynamic range of both ONU1 and ONU2 are kept stable at 10 dB.

IV. Conclusion

In this article, we have presented a dispersion compensation technique based on digital reservoir-computing for DFMA PON. Theoretical model of uplink of DFMA PON and RC-based equalization have been demonstrated, and optimum RC hyper-parameters have been identified to achieve the lowest BER in uplink of DFMA PON. In addition, the filtering effect has been explored with various digital filter parameters. Results have been shown that the RC-based equalization cannot compensate the distortion effects induced by large roll-off factor and short filter length. Moreover, the transmission capacity have been explored by adaptive bit loading in each OFDM subcarrier. It has shown that the aggregated capacity can be improved by around 13 Gb/s from 10 km to 40 km, achieving increment more than 25%. Finally, the differential optical launch power range has been calculated, showing that RC-assisted DFMA PON can be extended to 6 dB with all four ONUs, greatly improving the PON performance robustness.

References

[1] Q. Wang et al., "Can LAN-Wavelength division multiplexing meet the evolution of B5G/6G terabit/s fronthaul networks?," in *Proc. IEEE Opt. Fiber Commun. Conf. Exhib.*, 2023, pp. 1–3.

[2] Y. Wei et al., "Demonstration of point-to-multipoint 100G coherent PON to support broadband access and B5G/6G mobile X-haul," in *Proc. IEEE Opt. Fiber Commun. Conf. Exhib.*, 2023, pp. 1–3.

[3] M. Bolea, R. P. Giddings, M. Bouich, C. Aupetit-Berthelemot, and J. M. Tang, "Digital filter multiple access PONs with DSP-Enabled software reconfigurability," *J. Opt. Commun. Netw.*, vol. 7, no. 4, pp. 215–222, 2015.

[4] W. Jin et al., "Experimental demonstration of hybrid OFDM-digital filter multiple access PONs for 5G and beyond networks," in *Proc.IEEE Conf. Lasers Electro-Opt.*, 2020, pp. 1–2.

[5] W. Jin et al., "Hybrid SSB OFDM-digital filter multiple access PONs," *J. Lightw. Technol.*, vol. 38, no. 8, pp. 2095–2105, Apr. 2020.

[6] Y. Dong, R. P. Giddings, and J. Tang, "Hybrid OFDM-digital filter multiple access PONs," *J. Lightw. Technol.*, vol. 36, no. 23, pp. 5640–5649, Dec. 2018.
[7] X. Duan, R. P. Giddings, S. Mansoor, and J. M. Tang, "Experimental demonstration of upstream transmission in digital filter multiple access PONs with real-time reconfigurable optical network units," *IEEE/OSA J. Opt. Commun. Netw.*, vol. 9, no. 1, pp. 45–52, Jan. 2017.
[8] G. Meslener, "Chromatic dispersion induced distortion of modulated monochromatic light employing direct detection," *IEEE J. Quantum Electron.*, vol. 20, no. 10, pp. 1208–1216, Oct. 1984.
[9] Y. Dong et al., "Comparison of DC-value method and Kramers–Kronig receiver in optical OFDM SSB-DD transmission," *IEEE Photon. J.*, vol. 14, no. 4, pp. 1–8, Aug. 2022.
[10] R. Bonk et al., "50G-PON: The first ITU-T higher-speed PON system," *IEEE Commun. Mag.*, vol. 60, no. 3, pp. 48–54, Mar. 2022.
[11] L. Gruner-Nielsen et al., "Dispersion-compensating fibers," *J. Lightw. Technol.*, vol. 23, no. 11, pp. 3566–3579, Nov. 2005.
[12] N. Litchinitser, B. Eggleton, and D. B. Patterson, "Fiber Bragg gratings for dispersion compensation in transmission: Theoretical model and design criteria for nearly ideal pulse recompression," *J. Lightw. Technol.*, vol. 15, no. 8, pp. 1303–1313, Aug. 1997.
[13] W. Shien and I. Djordjevic, *OFDM for Optical Communications*. Amsterdam, The Netherlands: Elsevier, 2009.
[14] A. J. Lowery and J. Armstrong, "Orthogonal-frequency-division multiplexing for optical dispersion compensation," in *Proc. IEEE Conf. Opt. Fiber Commun. Nat. Fiber Optic Engineers Conf.*, 2007, pp. 1–3.
[15] B. J. C. Schmidt, A. J. Lowery, and J. Armstrong, "Experimental demonstrations of electronic dispersion compensation for long-haul transmission using direct-detection optical OFDM," *J. Lightw. Technol.*, vol. 26, no. 1, pp. 196–203, Jan. 2008.
[16] O. E. Agazzi, D. E. Crivelli, and H. S. Carrer, "Maximum likelihood sequence estimation in the presence of chromatic and polarization mode dispersion in intensity modulation/direct detection optical channels," in *Proc. IEEE Int. Conf. Commun.*, 2004, pp. 2787–2793.
[17] M. Rubsamen, J. M. Gene, P. J. Winzer, and R.-J. Essiambre, "ISI mitigation capability of MLSE direct-detection receivers," *IEEE Photon. Technol. Lett.*, vol. 20, no. 8, pp. 656–658, Apr. 2008.
[18] J. Jignesh et al., "Transmitter-side Volterra filtering for increased dispersion tolerance in 56 Gbaud PAM-4 systems," in *Proc. IEEE Opt. Fiber Commun. Conf. Expo.*, 2018, pp. 1–3.
[19] M. Li and S. Wang, "End-to-end learning for chromatic dispersion compensation in optical fiber communication," *IEEE Commun. Lett.*, vol. 26, no. 8, pp. 1829–1832, Aug. 2022.
[20] M. Schädler, G. Böcherer, and S. Pachnicke, "Soft-demapping for short reach optical communication: A comparison of deep neural networks and Volterra series," *J. Lightw. Technol.*, vol. 39, no. 10, pp. 3095–3105, May 2021.
[21] S. Gaiarin et al., "High speed PAM-8 optical interconnects with digital equalization based on neural network," in *Proc. IEEE Asia Commun. Photon. Conf.*, 2016, pp. 1–3.
[22] M. Chagnon, B. Karanov, and L. Schmalen, "Experimental demonstration of a dispersion tolerant end-to-end deep learning-based IM-DD transmission system," in *Proc. IEEE Eur. Conf. Opt. Commun.*, 2018, pp. 1–3.
[23] B. Karanov, D. Lavery, P. Bayvel, and L. Schmalen, "End-to-end optimized transmission over dispersive intensity-modulated channels using bidirectional recurrent neural networks," *Opt. Exp.*, vol. 27, no. 14, pp. 19650–19663, 2019.
[24] F. D. Ros, S. M. Ranzini, H. Bülow, and D. Zibar, "Reservoir-computing based equalization with optical pre-processing for short-reach optical transmission," *IEEE J. Sel. Topics Quantum Electron.*, vol. 26, no. 5, pp. 1–12, Sep./Oct. 2020.
[25] K. Nakajima and I. Fischer, Eds., *Reservoir Computing: Theory, Physical Implementations, and Applications*. Singapore: Springer, 2021.
[26] S. M. Ranzini, R. Dischler, F. d. Ros, H. Bülow, and D. Zibar, "Experimental demonstration of optoelectronic equalization for short-reach transmission with reservoir computing," in *Proc. IEEE Eur. Conf. Opt. Commun.*, 2020, pp. 1–4.
[27] Y. Osadchuk, O. Jovanovic, and D. Zibar, "Reservoir computing-based multi-symbol equalization for PAM 4 short-reach transmission," in *Proc. Conf. Lasers Electro- Opt.*, 2023, paper STu4G.3.
[28] M. Bolea, R. P. Giddings, and J. M. Tang, "Digital orthogonal filter-enabled optical OFDM channel multiplexing for software-reconfigurable elastic PONs," *J. Lightw. Technol.*, vol. 32, no. 6, pp. 1200–1206, Mar. 2014.
[29] Y. Dong, E. Al-Rawachy, R. P. Giddings, W. Jin, D. Nesset, and J. M. Tang, "Multiple channel interference cancellation of digital filter multiple access PONs," *J. Lightw. Technol.*, vol. 35, no. 1, pp. 34–44, Jan. 2017.